

# The luminosity function of the fossil group RX J1552.2+2013 <sup>1</sup>

Claudia L. Mendes de Oliveira

Departamento de Astronomia, Instituto de Astronomia, Geofísica e Ciências Atmosféricas da USP, Rua do Matão 1226, Cidade Universitária, 05508-090, São Paulo, Brazil

oliveira@astro.iag.usp.br

Eduardo S. Cypriano

Southern Astrophysics Research Telescope, Casilla 603, La Serena, Chile and Laboratório Nacional de Astrofísica, CP 21, 37500-000 Itajubá - MG, Brazil

ecypriano@ctio.noao.edu

Laerte Sodré Jr.

Departamento de Astronomia, Instituto de Astronomia, Geofísica e Ciências Atmosféricas da USP, Rua do Matão 1226, Cidade Universitária, 05508-090, São Paulo, Brazil

laerte@astro.iag.usp.br

## ABSTRACT

We determine the first fossil group luminosity function based on spectroscopy of the member galaxies. The fossil group RX J1552.2+2013 has 36 confirmed members, it is at a mean redshift of 0.136 and has a velocity dispersion of 623 km s<sup>-1</sup> (or 797 km s<sup>-1</sup> if four emission lines galaxies in the outskirts of the velocity distribution are included). The luminosity function of RX J1552.2+2013, measured within the inner region of the system ( $\sim 1/3 R_{vir}$ ), in the range  $-23.5 < M_{i'} < -17.5$ , is well fitted by a Schechter function with  $M_{i'}^* = -21.3 \pm 0.4$  and  $\alpha = -0.6 \pm 0.3$  or a Gaussian function centered on  $M_{i'} = -20.0 \pm 0.4$  and with  $\sigma = 1.29 \pm 0.24$  i' mag ( $H_0 = 70$  km s<sup>-1</sup> Mpc<sup>-1</sup>,  $\Omega_M=0.3$ ,  $\Omega_\Lambda=0.7$ ). The luminosity function obtained from a photometric survey in g', r', i'-bands (and statistical background correction) confirms the spectroscopically determined results. There is a significant dip in the luminosity function at  $M_{r'} = -18$  mag, as also observed for other clusters. RX J1552.2+2013 is a rich, strongly red-galaxy dominated system, with at least 19 galaxies with magnitudes between  $m_3$  and  $m_3 + 2$ , within a surveyed circular area of radius  $625 h_{70}^{-1}$  kpc centered on the peak of the x-ray emission. Its mass,  $\sim 3 \times 10^{14}$  M<sub>⊙</sub>, M/L of  $507 M_\odot/L_B$  and L<sub>X</sub> of  $6.3 \times 10^{43} h_{50}^{-2}$  ergs s<sup>-1</sup> (bolometric) are more representative of a fossil cluster than of a fossil group. The central object of RX J1552.2+2013 is a cD galaxy which may have accreted the more luminous ( $\sim L^*$ ) former members of the group. Although dynamical friction and subsequent merging are probably the processes responsible for the lack of bright galaxies in the system, for the fainter members, there must be another mechanism in action (perhaps tidal disruption) to deplete the fossil group from intermediate-luminosity galaxies ( $M_{r'} \sim -18$ ).

*Subject headings:* cosmology: observations – galaxies: clusters: individual: RX J1552.2+2013 – galaxies: elliptical and lenticular, cD – galaxies: evolution – galaxies: luminosity function, mass function – galaxies: kinematics and dynamics

## 1. Introduction

A fossil group is a system with a large extended X-ray halo, dominated by one brighter-than- $L^*$  elliptical galaxy which is surrounded by low-luminosity companions (where the difference in magnitude between the bright dominant elliptical and the next brightest companion is  $> 2$  mag). The first system identified as a fossil group was RXJ1340.6+4018, at a redshift of 0.171 (Ponman et al. 1994). A few years later, Vikhlinin et al. (1999) catalogued four systems which they called “X-ray overluminous elliptical galaxies”, given the unusually extended X-ray halos observed for what seemed to be isolated objects. These had essentially the same properties as fossil groups (in fact one of the four systems was the prototype fossil group from Ponman et al. 1994). Subsequently, Jones et al. (2003) catalogued five other fossil groups, selected from the WARPS survey. More recently, Yoshioka et al. (2004) catalogued four nearby systems (of which one is not a fossil group, namely RX J0419.6+0225 is the rich group NGC 1550). A few other individual fossil groups were recently catalogued: Khosroshahi et al (2004), Sun et al. (2004) and Ulmer et al. (2005) presented detailed X-ray studies of three additional fossil groups, NGC 6482, ESO 3060170 and Cl 1205+44, respectively. In total, there are then 15 known fossil groups catalogued to date (see Table 4). The X-ray halo of a fossil group is comparable in luminosity and extension to that of a rich group or poor cluster, suggesting that their masses may also be similar. Such systems are also thought to be quite abundant (their density is  $\sim 2.4 \times 10^{-7} \text{ Mpc}^{-3}$ , Jones et al. 2003) and therefore they may yield an important contribution to the luminosity density and to the baryon budget of the universe.

The main scenario for the formation of fossil groups is that they are possibly the successors of

massive versions of today’s compact groups (*merging origin*, Jones et al. 2003). In such a scenario, the brightest galaxies of the system would have merged, leaving behind a group/cluster dominated by a single elliptical galaxy, surrounded by small companions. On the other hand, a recent X-ray study by Yoshioka et al. (2004) points out that the M/L of four fossil groups studied by them reach up to  $M_{200}/L_B = 1100 \text{ M}_\odot/\text{L}_\odot$ , being at least one order of magnitude higher than the typical M/L for groups/clusters of galaxies of similar mass, which makes it very unlikely that fossil groups could be descendants of groups/clusters. However, other recent works derive much lower values of M/L for other such systems (e.g. Sun et al. 2004) and therefore this matter is not yet settled. In addition, it is possible that there is more than one formation mechanism for fossil groups. In the formation scenario proposed by Yoshioka et al. (2004), fossil groups are the massive end of the elliptical galaxy distribution, formed at high redshift (*fossil-elliptical origin*).

In a recent paper, D’Onghia & Lake (2004), based on the luminosity function of one such group, pointed out that fossil groups may pose a severe problem for the cold dark matter models. They pointed out that these systems do not have as much substructure as expected for such a massive system, and moreover the “missing galaxies” are much more luminous than those lacking in poor groups and in the field. However, the luminosity function of one fossil group in which that conclusion is based has been determined through imaging of the group and statistical background subtraction (Jones et al. 2000), with very few known redshifts. In fact, most of the past studies about fossil groups focused on their X-ray properties and very little information on their optical properties is available. In this paper, we present the first secure luminosity function determination of a fossil group, using spectroscopic data obtained with GMOS (Hook et al. 2002) on the Frederick C. Gillett Telescope (Gemini North) at Mauna Kea.

We present a spectroscopic study of RX J1552.2 +2013, one of the groups originally catalogued by Jones et al. (2003), selected from an X-ray survey done with ROSAT (WARPS) with well defined selection criteria. This system has high bolometric X-ray-luminosity ( $6.3 \times 10^{43} \text{ h}_{50}^{-2} \text{ ergs}^{-1}$ , Jones et al. 2003) and, before this study, it had one

---

<sup>1</sup>Based on observations obtained at the Gemini Observatory, which is operated by the Association of Universities for Research in Astronomy, Inc., under a cooperative agreement with the NSF on behalf of the Gemini partnership: the National Science Foundation (United States), the Particle Physics and Astronomy Research Council (United Kingdom), the National Research Council (Canada), CONICYT (Chile), the Australian Research Council (Australia), CNPq (Brazil) and CONICET (Argentina) – Observing run ID: GN-2004B-Q-47.

of the largest number of known members (four). We determine the luminosity function of the group from  $g'$ ,  $r'$ ,  $i'$  photometry down to  $i'=23$  and spectroscopy of 36 members. Sections 2 and 3 describe the observations, the reduction procedure and the results. In Section 3 we include, in Table 4, a summary of the main properties of the 15 known fossil groups to date. In section 4 we discuss the implications of our results for the understanding of the nature and evolution of fossil groups.

When needed, we adopt the following values for the cosmological parameters:  $H_0 = 70 \text{ km s}^{-1} \text{ Mpc}^{-1}$ ,  $\Omega_M=0.3$ , and  $\Omega_\Lambda=0.7$ .

## 2. Observations and reductions

The imaging and multi-slit spectroscopic observations of the group RX J1552.2+2013 were done with the GMOS instrument, mounted on the Gemini North telescope, on Aug 8th and Sep 9th/2004 respectively.

The imaging consisted of  $3 \times 200$ s exposures in each of the three filters from the SDSS system (Fukugita et al. 1996)  $g'$ ,  $r'$  and  $i'$ . The typical FWHM for point sources was  $\sim 0.75''$  in all images. All observations were performed in photometric conditions. Fig. 1 displays the  $r'$  image of the system.

The calibration to the standard SDSS system was made with the general extinction coefficients provided by the Gemini observatory <sup>2</sup>. The accuracy of the calibration is claimed to be within 5% to 8%.

Standard reduction using the Gemini package GMOS was used. After flat fielding and cleaning the images for cosmic rays, the final frames were analyzed with the program SExtractor (Bertin & Arnouts 1996). Positions and magnitudes (isophotal and aperture) were obtained for all objects. We estimate that the galaxy catalog is essentially complete down to  $23.5$   $i'$  magnitude, since the number counts turn over at  $i'=24$  mag.

Candidates for spectroscopy were chosen based on the color-magnitude diagram shown in Fig. 2: most of the galaxies with  $M_i < -20$ , below the red sequence (see continuous line in the figure) were observed spectroscopically. Galaxies above this line are expected to be in the background, since

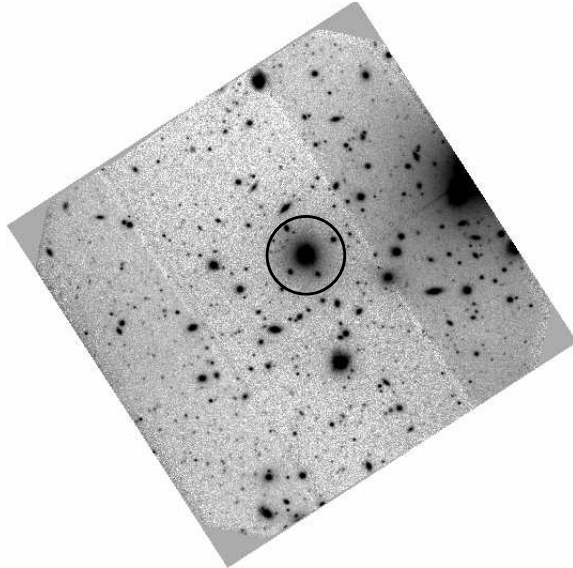


Fig. 1.— Optical image of RX J1552.2+2013. The field of view is 5.6 arcmin on a side, or  $803 h_70^{-1}$  kpc at the object redshift. North is up and east is to the left. The circle indicates the isophote where the surface brightness of the galaxy is equal to one sigma of the sky

their colors are redder than the expected colors of elliptical galaxies at the group redshift. Note that the outermost observed galaxy which turned out to be a member of the group/cluster has a distance of  $625 h_70^{-1}$  kpc from the X-ray center of RX J1552.2+2013.

One single multi-slit exposure of 100 minutes was obtained through a mask with  $1.0''$  slits, using the R400 grating, for a final resolution of  $8 \text{ \AA}$  (as measured from the FWHM of the arc lines), covering approximately the range  $4000 - 8000 \text{ \AA}$  (depending on the position of each slitlet). The spectra of three selected galaxies (from the best to the worst signal to noise) are shown in Fig. 3. Only four emission-line galaxies turned out to be members of the fossil-group. Most of them lie in the outskirts of the galaxy velocity distribution (see Table 1).

Standard procedures were used to reduce the multi-slit spectra using tasks within the Gemini IRAF <sup>3</sup> package. Wavelength calibration was

<sup>2</sup>[www.gemini.edu/sciops/instruments/gmos/gmosPhotStandards.htm](http://www.gemini.edu/sciops/instruments/gmos/gmosPhotStandards.htm) Observatories, which are operated by the Association of

done using Cu-Ar comparison-lamp exposures before and after the exposure.

Redshifts for galaxies with absorption lines were determined using the cross-correlation technique (Tonry & Davis 1979) as implemented in the package RVSAO (Kurtz & Mink 1998) running under IRAF. The final heliocentric velocities of the galaxies were obtained by cross-correlation with several template spectra. The final errors on the velocities were determined from the dispersion in the velocity estimates using several different galaxy and star templates. In the case of the three emission-line redshifts, the error was estimated from the dispersion in redshifts obtained using different emission lines. The resulting heliocentric velocities typically have estimated rms errors between 25 and 100 km s<sup>-1</sup>. The S/N of the data, measured at the continuum region around 6000–6300Å, ranged from 10 to 30.

Table 1 lists positions, isophotal magnitudes, aperture ( $g' - i'$ ) colors, radial velocities and the Tonry & Davis cross-correlation coefficient  $R$  for all galaxies with reliable velocity determination obtained in this study.

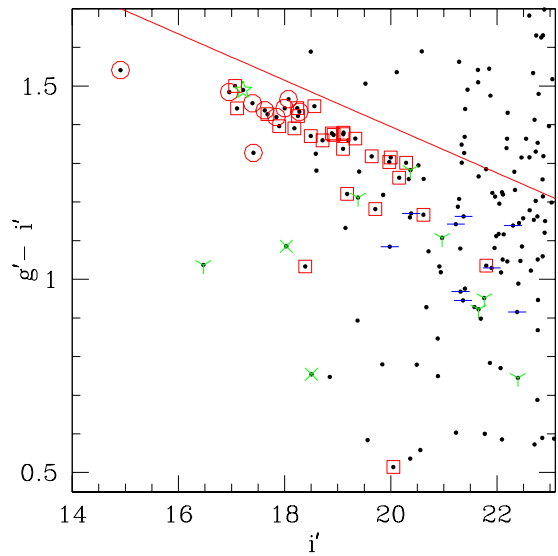


Fig. 2.—Color-magnitude diagram of the galaxies in the RX J1552.2+2013 field. Points marked with squares (members), ‘Y’ (non-members) and ‘-’ (with spectra but no redshift) represent the galaxies observed spectroscopically by us with GMOS-N. The circles (members), ‘x’ (non-members) and stars (doubtful cases) represent galaxies observed by Jones (2004, priv. comm.). The line indicates an upper limit for the cluster red-sequence we adopted when selecting the spectroscopic targets.

---

Universities for Research in Astronomy, Inc., under cooperative agreement with the National Science Foundation.

TABLE 1  
SPECTRAL DATA FOR GALAXIES IN THE RX J1552.2+2013 FIELD.

(1) Name	(2) RA (2000)	(3) DEC (2000)	(4) i' (AB Mag.)	(5) g'-i'	(6) Vel. (km s <sup>-1</sup> )	(7) R
G04.5+1221 <sup>a</sup>	15 52 04.5	+20 12 21	19.38	1.21	26819 ± 32	... <sup>b</sup>
G16.4+1605	15 52 16.4	+20 16 05	16.47	1.04	26820 ± 18	... <sup>b</sup>
G12.2+1439	15 52 12.2	+20 14 39	18.49	1.37	38715 ± 25	6.3
G23.2+1452	15 52 23.2	+20 14 52	20.05	0.51	39290 ± 36	... <sup>b</sup>
G10.0+1342	15 52 10.0	+20 13 42	20.61	1.17	39374 ± 100	... <sup>b</sup>
G12.2+1534	15 52 12.2	+20 15 34	18.18	1.39	39538 ± 43	7.3
G06.4+1406	15 52 06.4	+20 14 06	19.71	1.18	39765 ± 100	3.2
G06.8+1312	15 52 06.8	+20 13 12	17.07	1.50	40103 ± 34	10.2
G09.4+1157	15 52 09.4	+20 11 57	18.72	1.36	40115 ± 46	6.4
G10.9+1224	15 52 10.9	+20 12 24	21.80	1.03	40206 ± 59	2.8
G12.9+1305	15 52 12.9	+20 13 05	19.33	1.36	40211 ± 48	5.2
G16.0+1009	15 52 16.0	+20 10 09	17.10	1.44	40227 ± 45	5.9
G15.9+1211	15 52 15.9	+20 12 11	19.10	1.34	40305 ± 44	5.6
G11.9+1234	15 52 11.9	+20 12 34	19.10	1.38	40344 ± 39	5.8
G08.7+1136	15 52 08.7	+20 11 36	18.24	1.44	40472 ± 56	6.7
G05.9+1246	15 52 05.9	+20 12 46	19.18	1.22	40704 ± 47	3.2 <sup>c</sup>
G15.9+1039	15 52 15.9	+20 10 39	17.68	1.43	40748 ± 39	6.5
G17.0+1406	15 52 17.0	+20 14 06	20.00	1.32	40853 ± 66	4.1
G18.6+1410	15 52 18.6	+20 14 10	19.64	1.32	41001 ± 98	4.1
G16.8+1208	15 52 16.8	+20 12 08	19.97	1.30	41126 ± 87	3.3
G14.9+1404	15 52 14.9	+20 14 04	18.25	1.42	41142 ± 24	7.4
G10.5+1610	15 52 10.5	+20 16 10	17.90	1.40	41187 ± 35	7.2
G14.4+1115	15 52 14.4	+20 11 15	20.16	1.26	41275 ± 40	3.5
G11.4+1509	15 52 11.4	+20 15 09	20.29	1.30	41503 ± 96	2.4
G07.6+1439	15 52 07.6	+20 14 39	18.92	1.37	41582 ± 45	5.9
G16.9+1531	15 52 16.9	+20 15 31	18.89	1.38	41609 ± 48	6.6
G10.7+1519	15 52 10.7	+20 15 19	19.11	1.38	41797 ± 97	3.8
G13.2+1326	15 52 13.2	+20 13 26	18.56	1.45	42041 ± 48	7.2
G07.8+1503	15 52 07.8	+20 15 03	18.39	1.03	42045 ± 74	... <sup>b</sup>
G18.8+1345	15 52 18.8	+20 13 45	20.97	1.11	49262 ± 54	2.0
G11.4+1359	15 52 11.4	+20 13 59	20.37	1.28	68668 ± 40	4.5
G10.6+1139	15 52 10.6	+20 11 39	21.76	0.95	93209 ± 64	... <sup>b</sup>
G12.8+1516	15 52 12.8	+20 15 16	21.65	0.92	101640 ± 56	... <sup>b</sup>
G07.4+1239	15 52 07.4	+20 12 39	22.40	0.75	105743 ± 101	... <sup>b</sup>

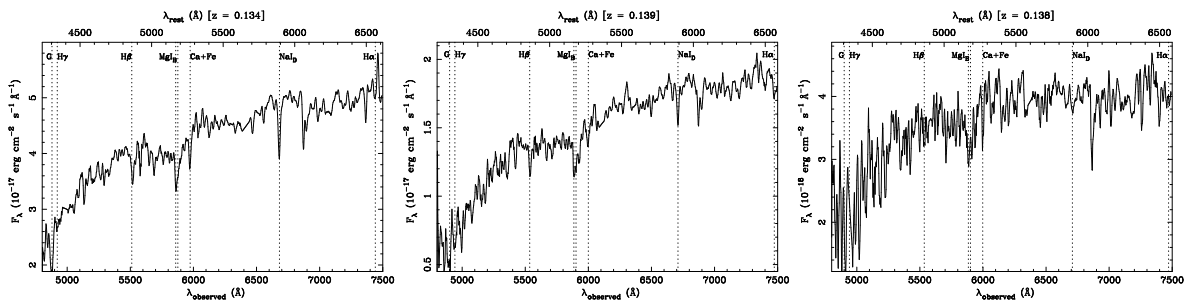


Fig. 3.— Spectra of member galaxies. The panels show, from left to right, spectra of galaxies G06.8+1312, G07.6+1439 and G11.4+1509 as examples of the data taken for this study. These spectra are the ones for which the largest, median and lowest cross-correlation coefficient was measured, respectively. The wavelength range used for the cross-correlation (4800–7500Å) is shown. In this figure, the spectra have been smoothed using a boxcar filter of size 13.6 Å (5 pixels), for the sake of clarity.

<sup>a</sup>The names of the galaxies are based on their 2000 celestial coordinates (RA seconds and DEC minutes and seconds). Thus galaxy Gab.c+defg is located at 15 52 ab.c +20 de fg.

<sup>b</sup>Redshift measured from emission lines.

<sup>c</sup>Redshift measured from absorption lines but it also has emission lines in the spectrum.

### 3. Results

#### 3.1. Galaxy velocity distribution

Using the heliocentric radial velocities listed in Table 1, we define the putative members of RX J1552.2+2013 as the 27 galaxies with velocities between 38715 and 42045 km s<sup>-1</sup>. There are nine other confirmed members studied by Jones et al. (private communication) which were included in most of our analysis, but not in the galaxy velocity distribution and determination of dynamical mass.

The data were analyzed with the statistical software ROSTAT (Beers, Flynn & Gebhardt 1990), which did not find any large gap in the velocity distribution. In addition, no other data-points were found outside a  $\pm 3\sigma$  range. Fig. 4 shows the velocity histogram for the 27 member galaxies studied by us.

Using the robust bi-weighted estimator, ROSTAT, the following values for the systemic redshift and velocity dispersion were found:  $\langle z \rangle = 0.1357 \pm 0.0011$  and  $\sigma = 797 \pm 185$  km s<sup>-1</sup>, respectively.

It is interesting to note, however, the effect of the exclusion of the emission-line galaxies when deriving these quantities, since those objects are believed to be recently accreted by the cluster, thus not yet virialized (e.g. Sodré et al. 1989; Biviano et al. 1997). Indeed, a simple inspection of Table 1 shows that 3 out of 4 emission-line galaxies occupy the edges of the velocity distribution.

The exclusion of the emission-line galaxies reduces the velocity dispersion of the group. As a consequence, the radial velocity for one other galaxy, G12.2+1439 falls outside the new  $\pm 3\sigma$  range. If this galaxy is also excluded, the new subsample is then composed of 22 galaxies, for which the bi-weighted values are  $\langle z \rangle = 0.136 \pm 0.001$  and  $\sigma = 635 \pm 164$  km s<sup>-1</sup>. We consider this determination of redshift and velocity dispersion the most reliable ones for RX J1552.2+2013 (see below). Note that for the determination of the luminosity function all 36 galaxies in the sample were used (including the ones with emission lines).

##### 3.1.1. Dynamical mass

We determine the dynamical mass of the cluster by using four different mass estimators, as sug-

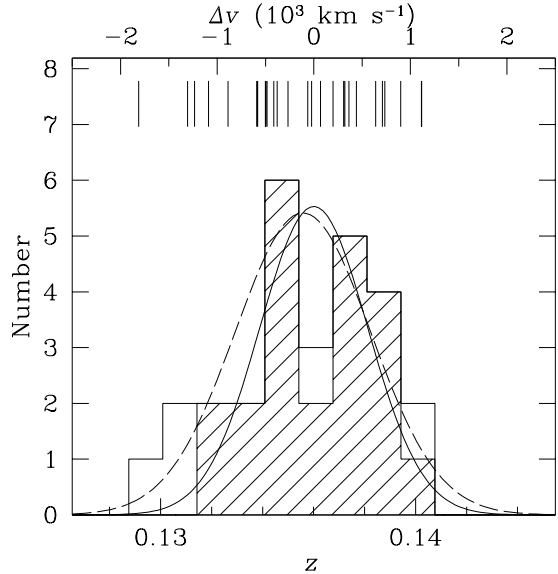


Fig. 4.— Velocity histogram of RX J1552.2+2013. It shows the distribution of the radial velocities of 27 galaxies in the inner  $625 h_{70}^{-1}$  kpc radius of RX J1552.2+2013, with redshifts within  $\pm 2500$  km/s of the systemic velocity of the group. The sticks on the upper part of the plot show velocities of individual objects. The ROSAT bi-weighted estimator gives a velocity dispersion  $\sigma = 797$  km/s and a redshift of  $\langle z \rangle = 0.1357$  (dashed line), for the sample of 27 objects. The dashed part shows a sub-sample of 22 galaxies, obtained by excluding four galaxies with emission lines and one other galaxy that becomes a  $\pm 3\sigma$ -outlier with this exclusion. The bi-weighted estimator returned  $\sigma = 635$  km/s and  $\langle z \rangle = 0.136$  (continuous line) for this smaller subsample.

gested by Heisler et al. (1985): virial, projected, average and median mass estimators (see Table 2).

The maximum difference between different mass estimates is about 24%. According to Heisler et al. there is a 75% chance that the derived mass of any single system is within a factor of order 2 of the correct value. However, caution notes have been given by several authors (e.g. Girardi & Mezzetti 2001) on the reliability of mass determinations when the galaxies are distributed over a small (central) part of the cluster and the number of redshifts is limited. The final, adopted mass for the cluster was obtained from the average value of

TABLE 2  
MASS ESTIMATES

(1) Estimator	(2) Mass ( $10^{14} M_{\odot}$ )	(3) M/L <sub>B</sub> ( $M_{\odot}/L_{B\odot}$ )	(4) All galaxies	
			Mass ( $10^{14} M_{\odot}$ )	M/L <sub>B</sub> ( $M_{\odot}/L_{B\odot}$ )
Virial	2.64	521	4.11	811
Projected	2.73	539	4.10	809
Average	2.20	433	3.29	649
Median	2.71	534	3.74	738
Mean value	2.57	507	3.81	752

the results of the four different estimators.

### 3.1.2. Location in the $L_X$ – $\sigma$ relation

The measured value of the bolometric X-ray luminosity of RX J1552.2+2013 is  $6.31 \times 10^{43} h_{50}^{-2}$  ergs $^{-1}$  (Jones et al. 2003) and there is no available measurement of  $T_X$  in the literature. This value of  $L_X$  is slightly above the value found for groups,  $L_X \lesssim 4 \times 10^{43} h_{50}^{-2}$  ergs $^{-1}$  and  $\sigma \lesssim 600$  km s $^{-1}$  (Xue & Wu 2000), being more consistent with a low-mass cluster.

According to the relations for groups and clusters from Mahdavi & Geller (2001), we find that for a system with this X-ray luminosity we would expect a velocity dispersion of about  $\sigma = 534$  km s $^{-1}$ , in good agreement with our direct measurement. In fact, even the value for the velocity dispersion calculated including emission-line galaxies (797 km s $^{-1}$ ) is within the dispersion of the points in their Fig. 1–(b).

The characterization of RX J1552.2+2013 as a cluster is also supported by the richness of this system. Within  $625 h_{70}^{-1}$  kpc of the central galaxy there are 19 galaxies between  $m_3$  (magnitude of the third brightest member) and  $m_3 + 2$ . The Abell, Corwin & Olowin (1989) definition for a cluster is at least 30 galaxies within a radius of 1.5 Mpc. Given the high density of observed members, this selection criterium would certainly have been fulfilled, had we surveyed a larger area.

### 3.1.3. Mass-to-light ratio

We estimated the luminosity of the central regions of the group by adding up the luminosities of the 36 spectroscopically confirmed members, taking into account the completeness correction derived from the spectroscopic sampling (see Fig. 5). The completeness correction was defined in the following way:  $N(m) = N_{grp}(m)/C(m)$ , where  $N_{grp}$  is the number of galaxies spectroscopically confirmed as members in a given magnitude bin.  $C(m)$  is the completeness, defined as:  $N_{vel}(m)/N_{tot}(m)$ , the number of galaxies in a given magnitude bin for which we were able to get a reliable redshift, over the total number of galaxies in the same magnitude bin. We note that, for this analysis, we have neglected all the galaxies redder than the red-cluster sequence, shown in Fig. 2.

In order to compare with previous results, we have transformed our SLOAN g' and r' magnitudes in standard Johnson–Morgan B magnitude using the transformations given in Fukugita et al. (1996). The total magnitudes have been corrected for Galactic extinction (Schlegel, Finkbeiner & Davis 1998) as well as for the  $k$ -correction (Fukugita, Shimasaku & Ichikawa 1995), under the assumption that all galaxies are early-type, which is valid for most of them.

The total luminosity calculated within  $625 h_{70}^{-1}$  kpc is  $5.06 \times 10^{11} M_{\odot} B$ . This leads to a mass-to-light ratio in units of  $M_{\odot}/L_{B\odot}$  of 507. Results for the several mass estimates and for the samples with and without emission-line galaxies are

presented in Table 2.

### 3.2. The Luminosity Function

We show in Fig. 5 the luminosity function of RX J1552.2+2013 (solid circles) for galaxies with spectroscopically confirmed membership either obtained in this paper (27 galaxies) or given by Jones et al. (private communication, 9 galaxies), corrected for incompleteness. The absolute magnitudes were calculated after correcting the observed magnitudes for Galactic extinction and applying  $k$ -corrections. The selection function, also shown in Fig. 5, was calculated considering only galaxies bluer than the upper limit of the adopted red cluster sequence.

We have also estimated photometrically the luminosity function of RX J1552.2+2013 down to  $\sim 23$  mag, in the three bands (the photometric sample is complete at this magnitude) by adopting the following procedure. First, we consider only galaxies bluer than the limit of the red sequence in the color-magnitude diagram shown in Fig. 2. We then binned the magnitudes of these galaxies in 1.0 magnitude bins and subtracted from each bin the average number of field galaxies with colors also below the red-sequence line, taken from two control fields. The two high-galactic latitude empty fields used as control fields were obtained with the same telescope, instrument and filters (Boris et al. 2005, in preparation). The counts derived from the two fields are in good agreement among themselves and with those of the Hawaii HDF-N field (Capak et al. 2004). The errors in each bin of the luminosity function were computed assuming Poissonian statistics for both field and group counts. These photometric luminosity functions are also shown in Fig. 5 as open triangles. They are strikingly similar to the spectroscopic results (solid circles). Note, however, that the determination of the luminosity function using galaxy counts on and off the field is significantly more uncertain than the spectroscopic determination given cosmic variance.

The shape of the luminosity function is very similar in the three bands. However, it is somewhat unexpected: the number of galaxies in the group flattens and then decreases for magnitudes fainter than  $g' \sim 20$ ,  $r' \sim 19.5$  and  $i' \sim 19$ . This can be clearly seen in the histogram shown in Fig. 6, of the number of galaxies, per magnitude inter-

val, below the red-cluster sequence.

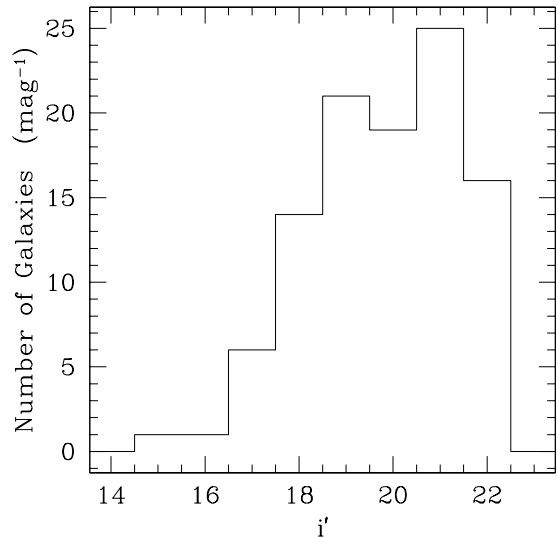


Fig. 6.— Number counts, per magnitude bin, below the red cluster sequence of RX J1552.2+2013 (i.e. below the continuous line in Fig. 2). Note that the number counts level off at the faint end indicating a flat or decreasing luminosity function for this system.

The shapes of the luminosity functions shown in Fig. 5 are well described by Gaussian functions. In the  $i'$ -band this Gaussian is centered at  $M_{i'} = -20.0 \pm 0.4$  ( $m_{i'} = 19.37$ ) and has  $\sigma = 1.29 \pm 0.3$  mag. If we attempt a fit with a Schechter function, the best parameters are, in the  $i'$ -band,  $M_{i'}^* = -21.3 \pm 0.5$  ( $m_{i'} = 18.05$ ) and  $\alpha = -0.59 \pm 0.24$ , in the range  $16 < m_{i'} < 22$ . Results for all bands and parameters for both Gaussian and Schechter luminosity functions are presented in Table 3. Note that the results for the spectroscopic luminosity function do not change significantly if we restrict the magnitude interval to exclude the faint magnitude bins which have one galaxy only (see results in middle pannel of Table 3). Lines indicating the best Schechter luminosity functions fitted first three lines of Table 3) are plotted in Fig. 5.

The results described above were checked in several ways. Here we exemplify the checks made, using the  $i'$ -band data, but equivalent results are obtained for the  $g'$ -band and  $r'$ -band data. The

TABLE 3  
LUMINOSITY FUNCTION

(1)	(2)	(3) Schechter Function	(4)	(5) Gaussian Function	(6)	(7)
	Band	$M^* + 5 \log(h_{70})$	$\alpha$	$\langle M \rangle + 5 \log(h_{70})$	$\sigma_M$	Magnitude range
Spectroscopic	$g'$	$-20.05 \pm 0.45$	$-0.42 \pm 0.32$	$-19.02 \pm 0.32$	$1.20 \pm 0.19$	18.0 – 23.0
	$r'$	$-21.07 \pm 0.48$	$-0.65 \pm 0.26$	$-19.59 \pm 0.41$	$1.31 \pm 0.25$	17.0 – 23.0
	$i'$	$-21.34 \pm 0.40$	$-0.59 \pm 0.29$	$-19.99 \pm 0.42$	$1.29 \pm 0.24$	16.0 – 22.0
Spectroscopic <sup>a</sup>	$g'$	$-20.35 \pm 0.58$	$-0.74 \pm 0.42$	$-19.01 \pm 0.50$	$1.21 \pm 0.27$	18.0 – 22.0
	$r'$	$-21.18 \pm 0.57$	$-0.77 \pm 0.37$	$-19.71 \pm 0.44$	$1.24 \pm 0.27$	17.0 – 21.0
	$i'$	$-21.38 \pm 0.44$	$-0.63 \pm 0.35$	$-20.10 \pm 0.42$	$1.23 \pm 0.24$	16.0 – 21.0
Photometric	$g'$	$-20.21 \pm 0.70$	$-0.47 \pm 0.42$	$-19.14 \pm 0.32$	$1.25 \pm 0.22$	17.0 – 23.0
	$r'$	$-21.27 \pm 0.62$	$-0.64 \pm 0.30$	$-19.82 \pm 0.36$	$1.31 \pm 0.27$	16.0 – 23.0
	$i'$	$-21.59 \pm 0.51$	$-0.67 \pm 0.27$	$-20.03 \pm 0.40$	$1.39 \pm 0.27$	15.0 – 23.0

<sup>a</sup>Note that these results have more limited magnitude range since bins with only one galaxy, at the faint end, were excluded

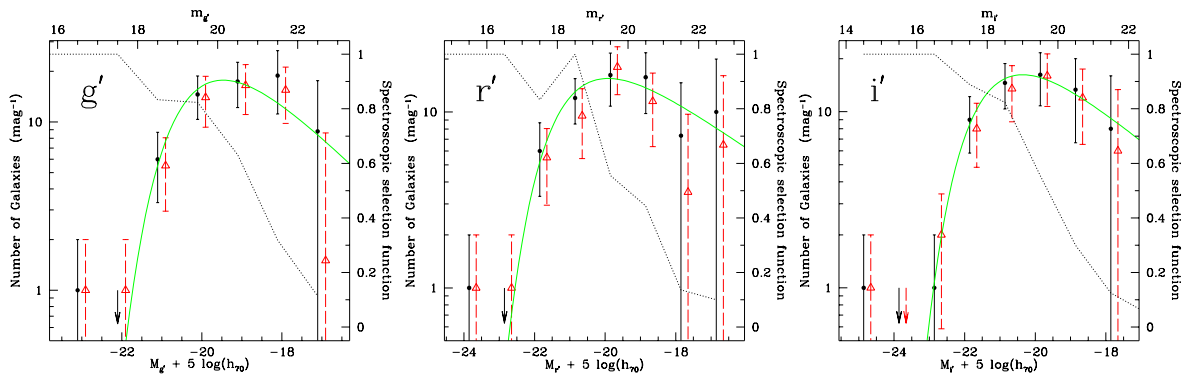


Fig. 5.— Luminosity Function of RX J1552.2+2013. The panels show, from left to right, the luminosity functions in the  $g'$ ,  $r'$  and  $i'$  bands, respectively. The solid circles show the completeness-corrected number of spectroscopically confirmed members of RX J1552 per 1.0 magnitude bin in the GMOS field. The error bars are  $1\sigma$  Poissonian errors. The arrows show bins with number of galaxies less or equal to zero. The dotted line is the selection function of the spectroscopic sample. The continuous lines show the best fitted Schechter function of the spectroscopic sample (see values in Table 3). The brightest galaxy of the cluster was not included in the fit. The open triangles show the photometrically-determined luminosity function estimated through number counts and statistical subtraction of the background. The points have been shifted by 0.2 mag, for the sake of clarity. The agreement between the spectroscopically and photometrically-determined luminosity functions is excellent.

number of galaxies brighter than  $i' = 22$  above the line in Fig. 2 which indicates the upper part of the red cluster sequence is 72 for RX J1552.2+2013 and  $64 \pm 7$  for the mean of the two control (empty) fields, indicating good agreement. Note that, above this line, the number of objects in the RX J1552.2+2013  $i'$  image and in the empty fields should match (apart, of course, from statistical fluctuations and cosmic variance) given that these are expected to reflect the numbers of background

objects. Moreover, if we plot a histogram of galaxy counts for objects below the cluster red sequence line (see Fig. 6), the histogram flattens for  $i' \gtrsim 20$ . Since the field counts increase continuously with magnitude, the number counts of group members decreases. Consequently, we are confident that the drop in the luminosity function of the group RX J1552.2+2013 is real.

Fossil groups have, by definition, a lack of bright galaxies because of the selection function

used to catalogue them. The bright-end of the luminosity function of these systems is then known to be unusual, with too few  $L^*$  galaxies. At the faint-end, nothing has been known, so far, about the shape of the luminosity function of these groups. For RX J1552.2+2013 we just reach the magnitude of the dwarf upturn (the point where the curve goes from being giant-dominated to dwarf-dominated), which in the Virgo cluster is around  $m_B = 17$ , corresponding to  $M_R = -18.5$ . Therefore, the steep downward slope at the faint-end of the luminosity function shown in Fig. 5 is in part due to the lack of dwarf galaxies in the sample. Such a pronounced dip in the luminosity function has already been observed in several other systems' luminosity functions and in particular in the composite luminosity function of compact groups studied by Hunsberger, Charlton & Zaritsky (2000). It is worth verifying whether this is a peculiarity of RX J1552.2+2013 or, otherwise, a common feature of fossil groups.

### 3.3. Surface photometry of the brightest cluster galaxy

In the upper panel of Fig. 7, the azimuthally averaged photometric profile of the central galaxy of RX J1552.2+2013 is shown. The surface photometry was performed using the task ELLIPSE in STSDAS/IRAF, which fits ellipses to extended object isophotes. We allowed the ellipticity and position angle of the successive ellipses to change but the center remained fixed. The ellipse fitting was performed only in the deeper  $r'$  image. For the other bands, the software measured the isophotal levels using the parameters estimated in the  $r'$  image. There were a few small objects within the outer isophotes of the central galaxy which were masked during the profile fitting procedure.

We have fitted a  $r^{1/4}$ -law to the bright end of the galaxy profile, from well outside the seeing disk ( $3.0''$ ) to a radius corresponding to  $\mu_{r'} = 23.0$  mag arcsec $^{-2}$  ( $8.3''$ ). In the lower panel of Fig. 7, the residuals (data –  $r^{1/4}$ -law model) for the  $r'$ -band data are shown. The light excess over the de-Vaucouleurs profile, which is clearly detected in all three filters, is interpreted here as due to an envelope. The presence of this light envelope, in addition to the high luminosity of the galaxy, strongly suggests that the central object of RX J1552.2+2013 is a cD galaxy.

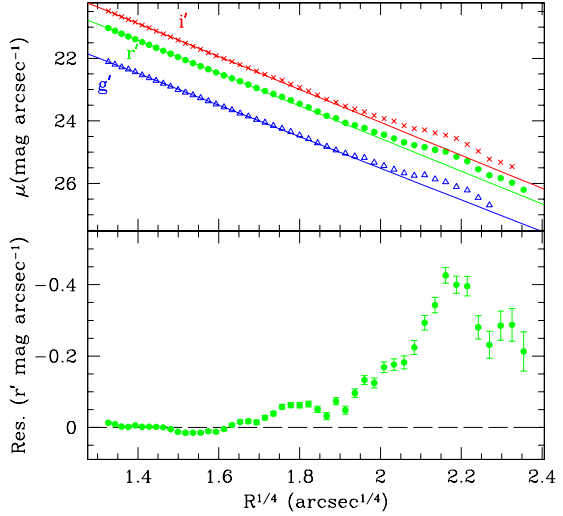


Fig. 7.— *Upper panel* Photometric profile of the central galaxy. We show the isophotal levels between a value of the semi-major axis of  $2.5''$  and that where the counts reach  $1\sigma$  of the background level ( $26.8$ ,  $26.3$  and  $25.6$  mag arcsec $^{-2}$  for  $g'$ ,  $r'$  and  $i'$  bands respectively) as a function of semi-major axis to the power  $1/4$ . The solid line is the best fit to the de Vaucouleurs profile between  $3.0$  and  $8.3''$  ( $\mu_{r'} = 23.0$  mag arcsec $^{-2}$ ). *Lower panel* residual between the actual  $r'$  band profile and the de Vaucouleurs profile fit to the bright end.

This result disagrees with a similar analysis done by Jones et al. (2003) using a profile which reached similar isophotal levels. On the other hand, we agree with Jones et al. (2003) that the subtraction of the best-fitting elliptical model does not reveal multiple-nucleus, shells or tidal tails.

## 4. Discussion

We list in Table 4 all fossil groups studied to date.

In Section 3.2 we showed that RX J1552.2+2013 has a luminosity function which has a dip at bright luminosities (by construction, since fossil groups were chosen to be environments with no bright elliptical galaxies besides the dominant elliptical) and, in addition, the luminosity function has a lack of faint galaxies around  $M_R = -18$ , just before the dwarf upturn, as seen in other systems such as for

TABLE 4  
FOSSIL GROUP GALAXIES KNOWN TO DATE

(1) Name	(2) RA (2000)	(3) DEC (2000)	(4) z	(5) $L_{X,bol}$ ( $10^{42} h_{50}^{-2}$ ) ergs $s^{-1}$	(6) Reference
NGC 1132	02 52 51.8	-01 16 29	0.0232	1.9	Yoshioka et al. (2004)
RX J0454.8-1806	04 54 52.2	-18 06 56	0.0314	1.9	Yoshioka et al. (2004)
ESO 306- G 017	05 40 06.7	-40 50 11	0.035805	129	Sun et al. (2004)
RX J1119.7+2126	11 19 43.7	+21 26 50	0.061	1.7	Jones et al. (2003)
RX J1159.8+5531	11 59 51.4	+55 32 01	0.0810	22	Vikhlinin et al. (1999)
CL 1205+44	12 05 53.7	+44 29 46	0.59	180	Ulmer et al. (2005)
RX J1256.0+2556	12 56 03.4	+25 56 48	0.232	61.	Jones et al. (2003)
RX J1331.5+1108	13 31 30.2	+11 08 04	0.081	5.9	Jones et al. (2003)
RX J1340.6+4018	13 40 33.4	+40 17 48	0.1710	25	Vikhlinin et al. (1999)
RX J1416.4+2315	14 16 26.9	+23 15 32	0.137	220.	Jones et al. (2003)
RX J1552.2+2013	15 52 12.5	+20 13 32	0.136	63	Jones et al. (2003)
NGC 6034	16 03 32.1	+17 11 55	0.0339	0.75	Yoshioka et al. (2004)
NGC 6482	17 51 48.8	+23 04 19	0.013129	2.17	Khosroshahi et al (2004)
RX J2114.3-6800	21 14 20.4	-68 00 56	0.1300	20	Vikhlinin et al. (1999)
RX J2247.4+0337	22 47 29.1	+03 37 13	0.199	41	Vikhlinin et al. (1999)

the Coma cluster. The faint end of the luminosity function of RX J1552.2+2013 is significantly different from that of other galaxy clusters of similar mass. Indeed, for the 2dF and RASS-SDSS clusters,  $\alpha \simeq 1.3$  in the blue-band (de Propris et al. 2003; Popesso et al. 2005), instead of values in the range  $-0.7$  to  $-0.4$  found here. In a search in the literature, we could find several examples of clusters which presented dips in their luminosity functions, but they are mostly associated with dense, dynamically well-evolved systems, such as X-Ray emitting cD clusters (e.g. Lopez-Cruz et al. 1997; Valotto et al. 2004; Mobasher et al. 2003). On the other hand, a few loose groups, like Leo I, has also been reported to have a dip in its luminosity function at intermediate luminosities (between  $-19.5 < M_R < -16$ ; Flint et al. 2003), and the luminosity function of compact groups of galaxies also show a similar dip (Hunsberger et al. 1996), which suggests that there may be more than one mechanism in action, for the depletion of these galaxies in different environments.

Fossil groups were suggested to be the end products of merging of  $L^*$  galaxies in low-density environments (Jones et al. 2003). The specific fossil group studied here, however, does not constitute a low-density environment and, in fact, is more similar to a galaxy cluster. The fairly high X-ray emission, the large fraction of elliptical galaxies (most of the bright galaxies in Fig. 1 are early-types), the radial velocity distribution (Fig. 4), as well as the lack of obvious substructures, suggest

that RX J1552.2+2013 is probably virialized.

Under the merger scenario hypothesis, the mechanism usually claimed to explain the lack of  $L^*$  galaxies is dynamical friction. It works by a deceleration of the orbital velocity of a galaxy, where the galaxy loses its kinetic energy to the pool of dark matter particles. This phenomenon causes the galaxy to spiral towards the mass center and eventually to merge with the central galaxy. The frictional deceleration is proportional to the mass of the galaxy, so this process is expected to be more efficient for the brightest cluster members. This process is probably more efficient during the cluster collapse- when radial orbits may prevail- than after virialization, when the galaxy orbits are more isotropic (e.g. Merritt 1985). Fossil groups/clusters appear to be an extreme case of this dynamical friction scenario, since all  $L^*$  galaxies have merged and there was no further accretion of bright field galaxies into the system.

Dynamical friction and subsequent merging are probably the processes responsible for the lack of bright galaxies in the luminosity function of fossil groups. However, it is interesting to note that these same physical processes cannot be efficient enough for low-mass galaxies in order to explain the shortage of low-luminosity galaxies (around  $M_R = -18$  mag).

An attractive explanation for the lack of faint galaxies in dense environments is the dimming or even total disruption of these objects caused by a succession of tidal encounters (Gnedin 2003). The

debris of the disruption of such galaxies is one of the possible sources of diffuse intra-cluster light and/or cD envelopes. Indeed, as shown in Section 3.3, the central galaxy of RX J1552.2+2013 has the light excess over its de Vaucouleurs profile that characterizes cD galaxies.

What is puzzling about fossil systems and RX J1552.2+2013 in particular is the high efficiency with which both mechanisms have acted. The general case for clusters is to not have dips in the luminosity functions (de Propis et al. 2003; Popesso et al. 2005). The exceptions are the central regions of rich clusters. For instance, the dip in the luminosity function of the Coma cluster core is at  $R \sim 17.0$  and  $B \sim 18.0$  (Trentham 1998), which is close to the faintest limit of the luminosity functions presented here.

On the other hand, the disruption of faint galaxies is not instantaneous, requiring a few crossing times before tidal heating can strip off less bound stars or even tear the galaxies apart. Therefore, the faint galaxies should be bound to these structures since pre-virialization times. Moreover, the existence of a very compact and rich core in this system should increase greatly the number of collisions, enhancing the tidal stripping efficiency.

If this scenario is correct, we should not expect the same lack of faint galaxies in less rich fossil groups, where the galaxy density and thus the tidal encounters were much less frequent at early times. More observations are needed to test this scenario.

One detail that should be kept in mind is that we have observed just the inner part of RX J1552.2+2013 ( $\sim 1/3 R_{vir}$ ), region where a few previous studies have found a lower dwarf-to-giant ratio than that measured in the outskirts of the systems (e.g. Phillipps et al. 1998). Popesso et al. (2005), however, using a very large sample of 130 SDSS clusters with X-ray counterparts, have found only a weak dependence of the dwarf-to-giant ratio with cluster-centric distance. The fundamental parameter, in this case, seems to be the local density (Driver, Couch & Phillipps 1998), instead of the cluster-centric distance. And, if we are to draw any conclusions based on the present knowledge of fossil systems and the data we gathered, is that fossil systems had a very dense origin.

Considering the merging scenario, it is possi-

ble that the overluminous galaxy has been formed within a substructure inside the already consolidated larger structure. In that case, one could think of a scenario where a compact group was formed within a larger rich group, which would then have quickly merged and would have left behind the brightest elliptical galaxy of what today is seen as a fossil group. One weak argument against this scenario is that compact groups are not usually found within such massive structures, but instead are more often surrounded by loose groups. This may, however, be a selection effect in the compact group catalogues available in the literature, which use an isolation criterion for group selection and may, therefore, select against compact groups embedded in clusters.

Another important point is that member galaxies in compact groups are emerging as very old systems (Proctor et al. 2004; Mendes de Oliveira et al. 2005). This suggests two possible scenarios for compact groups: they are either long-lived systems, which have not had a major merger over a significant fraction of a Hubble time (scenario also supported by Zabludoff & Mulchaey 1998) or they are systems which merge so fast that they are not caught at intermediate stages of evolution. The existence of a large population of fossil groups would support the latter scenario of fast merging for compact groups, at least for those within clusters or rich groups.

One problem for the *merging origin* of fossil groups is their apparent much higher mass-to-light ratios as compared to compact groups and poor clusters. As explained earlier, recent work of Yoshioka et al. (2004) derive very high values for the M/L of fossil groups and conclude that at least some fossil groups are not end products of compact group evolution. They suggest that alternatively these objects are the massive tail of the elliptical galaxy distribution, formed at high redshift (*fossil-elliptical origin*). In the present case, the system is definitely a cluster and not a single elliptical galaxy.

The whole scenario of fossil group formation may become more clear when more of these groups are studied spectroscopically. Ongoing determinations of the luminosity function for a large sample of fossil groups and the detailed study of the properties of the brightest group members, including the determination of their ages and metal abun-

dances, may also elucidate some of these questions. In addition, simulations such as those presented recently by D'onghia et al. 2005 (astro-ph/0505544), but at higher resolution, will allow a direct comparison of the observed luminosity function of a fossil group and the expected luminosity function of merged groups.

We are grateful to Laurence Jones and Natalia Boris, for granting us access to their data prior to publication. We would like to thank the Gemini staff for obtaining the observations, Elena D'Onghia, Daniele Pierini, Gastão Lima Neto, Simon Driver and Roberto de Propris for useful suggestions. The authors would like to acknowledge support from the Brazilian agencies FAPESP (projeto temático 01/07342-7), CNPq and CAPES. We made use of the Hyperleda database and the NASA/IPAC Extragalactic Database (NED). The latter is operated by the Jet Propulsion Laboratory, California Institute of Technology, under contract with NASA.

## REFERENCES

Abell, G. O., Corwin, H. G., Jr., Olowin, R. P. 1989, *ApJS*, 70 1

Beers, T. C., Flynn K. & Gebhardt 1990, *AJ*, 100, 32

Bertin, E. & Arnouts, S. 1996, *A&AS*, 117, 393

Biviano, A., Katgert, P., Mazure, A., Moles, M., den Hartog, R., Perea, J., Focardi, P. 1997, *A&A*, 321, 84

Capak, P., Cowie, L. L., Hu, E. M., Barger, A. J., Dickinson, M., Fernandez, E. et al. 2004, *AJ*, 127, 180

Driver, S. P., Couch, W. J., Phillipps, S., 1998, *MNRAS*, 301, 369

D'Onghia, E., Lake, G. 2004, *ApJ*, 612, 628

Flint, K., Bolte, M, Mendes de Oliveira 2003, *Ap&SS*, 285, 191

Fukugita, M., Shimasaku, K., Ichikawa, T. 1995, *PASP*, 107, 945

Fukugita, M., Ichikawa, T., Gunn, J. E., Doi, M., Shimasaku, K. & Schneider, D. P. 1996, *AJ*, 111, 1748

Girardi, M. & Mezzetti, M. 2001, *ApJ*, 548, 79

Gnedin, O. Y. 2003, *ApJ*, 589, 752

Hayashi, E., Navarro, J. F., Taylor, J. E., Stadel, J., Quinn, T. 2003, *ApJ*, 584, 541

Heisler, J., Tremaine, S., Bahcall, J. N. 1985, *ApJ*, 298, 8

Hook, Isobel, Allington-Smith, J. R., Beard, S., Crampton, D., Davies, R., Dickson, C. J., Ebbers, A., Fletcher, M., Jorgensen, I., Jean, I., Juneau, S., Murowinski, R., Nolan, R., Laidlaw, K., Leckie, B., Marshall, G.E., Purkins, T., Richardson, I., Roberts, S., Simons, D., Smith, M., Stilburn, J., Szeto, K., Tierney, C. J., Wolff, R. & Wooff, R. 2002, SPIE, 4841, Power Telescopes and Instrumentation into the New Millennium

Hunsberger, S. D., Charlton, J. C., Zaritsky, D. 2000, *ASP Conference Series*, 209, 81. Published by Astronomical Society of the Pacific, San Francisco, CA Mauri J. Valtonen and Chris Eds.

Ishizawa, T., Matsumoto, R., Tajima, T., Kageyama, H., Sakai, H. 1983, *PASJ*, 35, 61

Jones, L. R., Ponman, T. J., Forbes, Duncan A. 2000, *MNRAS*, 312, 139

Jones, L. R., Ponman, T. J., Horton, A., Babul, A., Ebeling, H., Burke, D. J. 2003, *MNRAS*, 343, 627

Khosroshahi, Habib G., Jones, Laurence R., Ponman, Trevor J. 2004, *MNRAS*, 349, 1240

Kurtz, M. J. & Mink, D. J. 1998, *PASP*, 110

Lopez-Cruz, O., Yee, H. K. C., Brown, J. P., Jones, C., Forman, W. 1997, *ApJ*, 475, 97, 934

Mahdavi, A., Geller, M.J. 2001, *ApJ*, 554, 129

Mendes de Oliveira, C., Coelho, P., Gonzalez, J.J., Barbuy, B. 2005, *astro-ph/0503098*

Merritt, D. 1985, *ApJ*, 289, 18

Mobasher, B., Colless, M., Carter, D., Poggianti, B., Bridges, T., Kranz, K. et al. 2003, *ApJ* 587, 605

Moore, B., Ghigna, S., Governato, F., Lake, G., Quinn, T., Stadel, J., Tozzi, P. 1999, ApJ, 524, 19

Phillipps, S., Driver, S. P., Couch, W. J., Smith, R. M. 1998, ApJ, 498, L119

Ponman, T. J., Allan, D. J., Jones, L. R., Merrifield, M., McHardy, I. M., Lehto, H. J., Lupino, G. A. 1994, Nature, 369, 462

Popesso, P., Böhringer, H., Romaniello, M., Voeges, W. 2005, A&A, 433, 415

Proctor, R. N., Forbes, D. A., Hau, G. K. T., Beasley, M. A., De Silva, G. M., Contreras, R., Terlevich, A.I. 2004, MNRAS, 349, 1381

De Propris, R. et al. 2003, MNRAS, 342, 725

Schlegel, S., Finkbeiner, D. P. & Davies, M. 1998, ApJ, 500, 525

Sodré, L., Jr., Capelato, H. V., Steiner, J. E., Mazure, A. 1989, AJ, 97, 1279

Sun, M., Forman, W., Vikhlinin, A., Hornstrup, A., Jones, C., Murray, S. S. 2004, ApJ, 612, 805

Tonry, J. & Davis, M. 1979, AJ, 84, 1511

Trentham, N. 1998, 293, 71

Ulmer, M.P., Adami, C., Covone G., Durret, F., Lima Neto G.B., Sabi rli, K., Holden, B., Kron, R.G., Romer, A.K., astroph 0501486, accepted in ApJ

Valotto, C. A., Muriel, H., Moore, B., Lambas, D. G. 2004, ApJ, 603, 67

Vikhlinin, A., McNamara, B. R., Hornstrup, A., Quintana, H., Forman, W., Jones, C., Way, M. 1999, ApJ, 520, 1

Xue, Y.-J., Wu, X.-P. 2000, ApJ, 538, 65

Yoshioka, T., Furuzawa, A., Takahashi, S., Tawara, Y., Sato, S., Yamashita, K., Kumai, Y. 2004, AdSpR, 34, 2525

Zabludoff, A. I., Mulchaey, J. S. 1998, ApJ, 498, 5